ISSN 0036-0244, Russian Journal of Physical Chemistry A, 2021, Vol. 95, No. 13, pp. 2653–2662. © Pleiades Publishing, Ltd., 2021.

PHYSICAL CHEMISTRY
OF SURFACE PHENOMENA

# Evaluation of Natural Montmorillonite Clay for Removal of $Cd^{2+}$ from Aqueous Solution in a Batch Adsorption System

**Soufiane Boudjemaa**[a,b,*]

[a] *Laboratory of Chemical Process Engineering, Ferhat Abbas Setif 1 University, Setif, Algeria*

[b] *Faculty of Sciences and Technology, Mohamed El Bachir El Ibrahimi B.B.A University, Bordj Bou Arréridj, Algeria*

**e-mail: bsouf77@yahoo.fr*

Received August 6, 2020; revised August 6, 2020; accepted November 13, 2020

**Abstract**—Montmorillonite clay (MMT) sample has been structurally characterized using different techniques such as XRD, FTIR, TGA, SEM, and EDX, and evaluated as a sorbent for $Cd^{2+}$ ions removal from aqueous solutions were studied in a batch adsorption system. The specific surface area (SSA) and cation exchange capacity (CEC) were determined using methylene blue test and they were found to be 177 $m^2/g$ and of 94 meq/100 g, respectively. The effect of parameters like pH value, contact time, initial $Cd^{2+}$ concentration and temperature was experimentally studied in batch mode. The extent of $Cd^{2+}$ adsorption increased with increasing initial concentration of adsorbat, pH, and temperature. The linear Langmuir and Freundlich models were applied to describe equilibrium isotherms and both models fitted well. The monolayer adsorption capacity for $Cd^{2+}$ ions was 12.30 mg/g at pH 6.1 and 25°C. Thermodynamic parameters showed that the adsorption of $Cd^{2+}$ onto montmorillonite clay was spontaneous and endothermic process. Furthermore, the Lagergren-first-order and pseudo-second-order models were used to describe the kinetic data. The experimental data fitted well the pseudo-second-order kinetics. As a result, the montmorillonite clay may be used for removal of $Cd^{2+}$ from aqueous media.

**Keywords:** montmorillonite, characterization, $Cd^{2+}$, adsorption isotherm, kinetic, thermodynamic

**DOI:** 10.1134/S0036024421130045

## INTRODUCTION

An enormous amount of toxic heavy metals is being discharged into the environment as a waste from batteries, tanneries, electroplating, pesticides, fertilizers, mining and ore refining industries [1]. Unlike other water pollutants, heavy metals tend to accumulate in living organisms resulting in potential risks to human health and environment [2]. Among heavy metals, cadmium have attracted special attention. For humans, cadmium is a carcinogen. It can also cause kidney damage [3]. The United States Environmental Protection Agency (USEPA) recommended that the maximum contamination level for cadmium in drinking water should not exceed 0.01 mg/L [4]. Therefore, the process of cadmium removal from bodies of water is very important and attracts the interest of many researchers.

Several methods and techniques have been proposed for cadmium ion removal including adsorption [5], precipitation [6], bioremediation [7], membrane filtration [8], ion-exchange [9], and solvent extraction [10]. However, these methods have several disadvantages/limitations such as being expensive, generating secondary pollutants like sludge, and are ineffective in treating effluents with low metal concentrations etc.

Among these techniques, adsorption was considered superior due to its high efficiency, easy operation, cost effectiveness and availability of efficient adsorbents [11]. Many adsorbents have been evaluated for cadmium ions uptake including clay minerals [12], activated carbon [13], zeolites [14], metal oxides [15], composites [16], functionalized polymers [17], and carbon nanotubes [18]. Due to their natural abundance, high sorption capacity and chemical and mechanical stability, clay minerals are considered substantial adsorbents. The sorption capacity of clays is imparted from a relatively high specific surface area and a net negative surface charge [19].

Montmorillonite, one of the most widely used clays, has been proven efficient in removal of heavy metals, including Cu, Pb, Co, Zn, and Cd, which is of great concern because of the increasing trend in discharge, stability in nature, and high toxicity [20, 21]. Montmorillonite is a clay belonging to the smectite clay group characterized by a 2 : 1 structure with one octahedral sheet of $Al^{3+}$ grid sandwiched between two tetrahedral sheets of $Si^{4+}$ (Fig. 1). Isomorphic substitu-

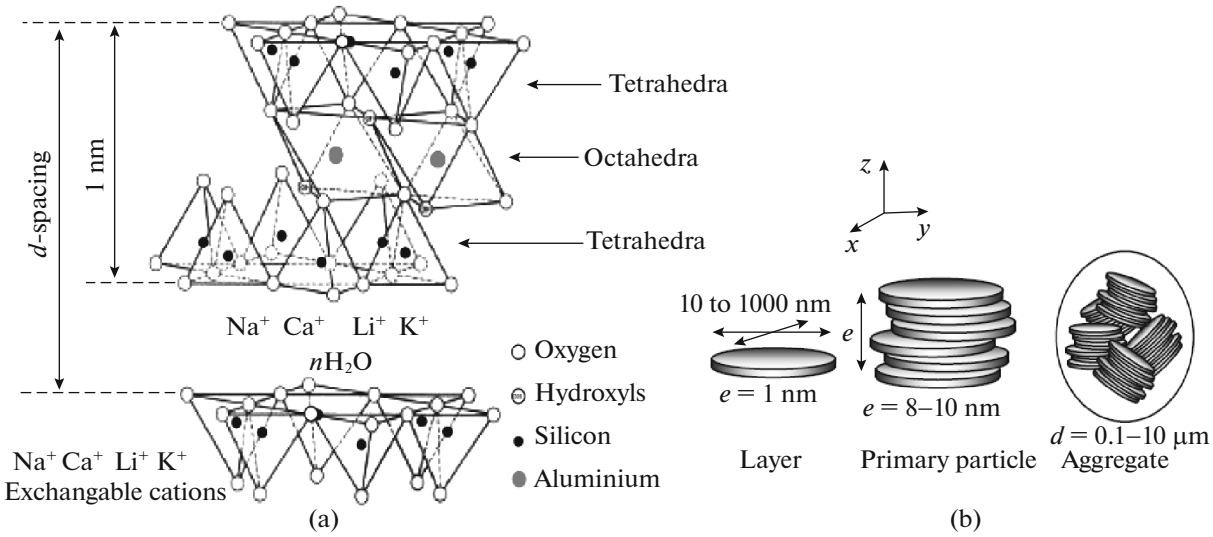


**Fig. 1.** Montmorillonite: (a) crystalline structure and (b) microstructure.

tions within the octahedral sheets produce a net negative surface charge [22, 23]. In recent decades, the applicability of montmorillonite from different regions for heavy metals removal has been studied extensively [24].

The objective of the present work is to study the adsorption characteristics of $Cd^{2+}$ ions from aqueous solution using montmorillonite clay. The influences of adsorption conditions such as contact time, pH changes, initial concentration of $Cd^{2+}$ ions and temperature effect were investigated. In addition, the physico-chemical characteristics of montmorillonite clay obtained by XRD, IR, TGA, SEM, and EDX were studied to understand the adsorption mechanism. Finally, the possibility to use montmorillonite clay to remove $Cd^{2+}$ metal ion from wastewater was demonstrated.

## EXPERIMENTAL

### *Materials*

Natural montmorillonite (MMT) was supplied by the County of Maghnia, Western Algeria, and used after purification. Cadmium chloride ($CdCl_2 \cdot H_2O$) is used as metal solution. This stock solution was then diluted to specified concentrations. The pH adjustment was carried out using 0.1 N hydrochloric acid (HCl) and 0.1 N sodium hydroxide (NaOH). Chemicals of analytical grade were purchased from Merck. All plastic sample bottles and glassware were cleaned, then rinsed with deionized water and dried at 60°C in a temperature controlled oven.

### *Montmorillonite Pretreatment*

Montmorillonite (MMT) clay (50 g) was placed in 750 mL vessel with distilled water and stirred for 2 h. The suspension was decanted and separated by centrifugation. This procedure was repeated four times. Finally, the precipitate (MMT) was oven dried at 120°C for 24 h and crushed. The chemical composition of dried sample is given in Table 1.

### *Batch Adsorption Experiments*

The adsorption measurements were performed using batch equilibrium technique at ambient temperature. The effect of contact time on the adsorption capacity of MMT was studied in the range 1–360 min at an initial concentration of 100 mg/L. Adsorption kinetics was studied using an initial concentration of 100 mg/L with the adsorbent dosage of 0.2 g/20 mL at pH 6.1. Adsorption isotherms were studied at various initial concentrations of $Cd^{2+}$ ion in the range of 10–120 mg/L and the experiments were conducted at different constant temperatures in the range 25–60°C. The $Cd^{2+}$ adsorption capacity of MMT in the batch test was calculated using following equations:

$$R_{\text{ratio}} = \left(\frac{C_0 - C_e}{C_0}\right) \times 100\%, \quad (1)$$

**Table 1.** Chemical composition (wt %) of initial MMT according to XRF analysis

| Others | $SiO_2$ | $Al_2O_3$ | $Fe_2O_3$ | $TiO_2$ | $P_2O_5$ | $SO_3$ | $K_2O$ | MnO | $ZrO_2$ | CaO |
|---|---|---|---|---|---|---|---|---|---|---|
| Balance | 71.60 | 12.75 | 10.77 | 1.66 | 0.70 | 0.09 | 0.09 | 0.02 | 0.04 | 0.31 |

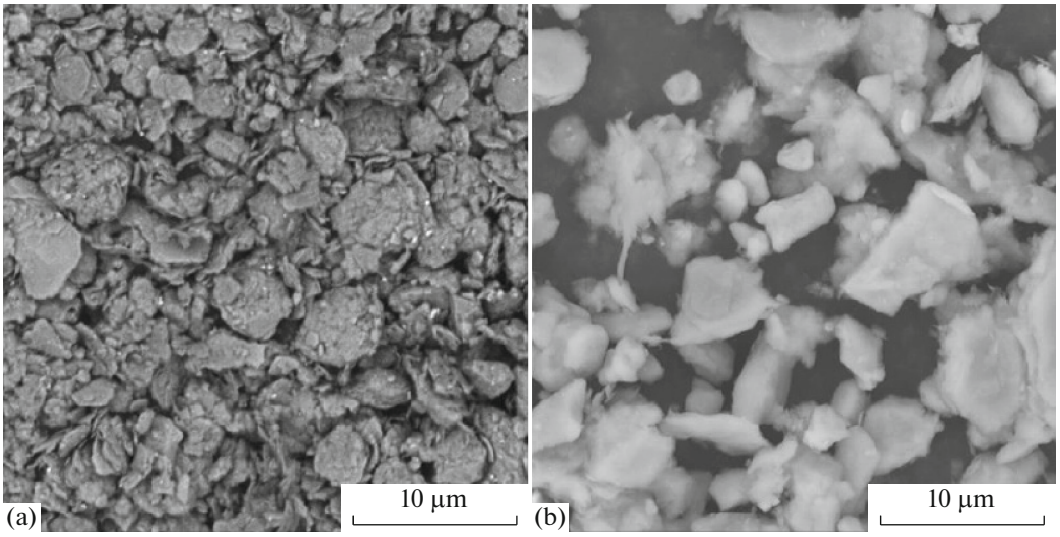


**Fig. 2.** SEM micrograph of: (a) MMT and (b) Cd-adsorbed MMT.

$$q_e = \frac{(C_0 - C_e)}{m} V, \quad (2)$$

where $R_{ratio}$ is the $Cd^{2+}$ removal rate, $q_e$ (mg/g) is the equilibrium capacity of $Cd^{2+}$ on the MMT, $C_0$ and $C_e$ (mg/L) are, respectively, the initial concentration and concentration at equilibrium of the $Cd^{2+}$ solution, $V$ (L) is the solution volume, and $m$ (g) is the mass of MMT. All assays were carried out in triplicate and the mean values are presented.

### *Characterization*

X-ray diffraction (XRD) measurements were carried out using Philips diffractometer (PW-1710) with Cu$K_\alpha$ ($\lambda = 1.54$ Å) radiation source operating at 40 kV and 30 mA at room temperature. All scans were performed in 2θ range 2°–20° with scan speed of 2 deg/min.

Chemical analysis was performed by X-ray fluorescence (XRF) spectroscopy on ElvaX Pro (Elvatech) spectrometer.

FTIR spectra of MMT were recorded using Shimadzu FTIR-8300 in the range of 400–4000 $cm^{-1}$, using KBr disc method.

The morphology of MMT was studied by scanning electron microscopy (SEM) (JSM-5900 LV).

The specific surface area (SSA) and cation exchange capacity of the MMT sample were determined by methylene blue titration and spot methods, respectively [25].

Concentrations of $Cd^{2+}$ ions in the solutions were measured using an AA-6300 atomic absorption spectrophotometer (Shimadzu, Japan).

Thermal gravimetric analysis (TGA) was conducted on a Shimadzu TGA-51H instrument in the temperature range from 30 to 900°C; heating rate of 10 K/min in nitrogen atmosphere with a purge rate of 20 mL/min.

## RESULTS AND DISCUSSION

### *Characterization of Sorbent*

**Scanning electron microscopy (SEM)** is an important tool used in the determination of the surface morphology of an adsorbent. In this study, SEM was used to reveal the change in morphological features of MMT and Cd-adsorbed MMT (Fig. 2).

The SEM results showed that the surface morphology of Cd-adsorbed MMT is different from that of natural MMT. The natural MMT showed loose aggregates with a porous structure. After adsorption, the surface of MMT demonstrates compacted aggregates. The surface morphology of the natural MMT changed evidently during the adsorption process, indicating that significant interaction at the cadmium–clay interface.

**IR spectroscopy.** FT-IR spectra provide useful information about the surface functional groups which affect the adsorption process. For this reason, the FT-IR spectrum of the MMT clay was recorded as shown in Fig. 3. As noted, all the spectra show bands at 3636 and 3395 $cm^{-1}$ attributed to O–H stretching for the silicate and water, respectively, 1631 $cm^{-1}$ (related to O–H bending), 1039 $cm^{-1}$ (owing to stretching vibration of Si–O–Si from silicate), 912 $cm^{-1}$ (from Al–OH–Al deformation of aluminates), 525 and 470 $cm^{-1}$ (Al–O stretching and Si–O bending vibrations of MMT, respectively), and 789 $cm^{-1}$ (related to Si–O stretching vibration) [26, 27].

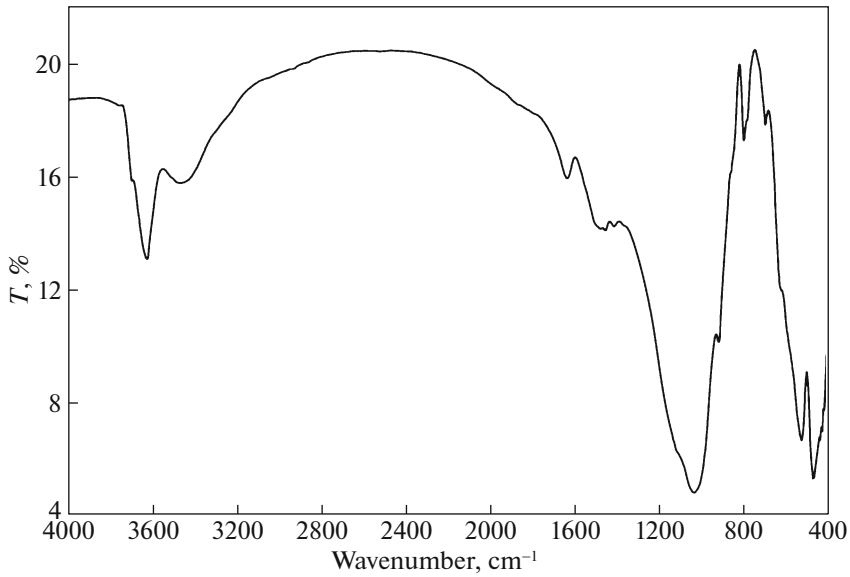


**Fig. 3.** FTIR spectra of MMT.

**XRD analysis** is widely used to investigate the mineralogical composition of clay minerals which deeply affects their physiochemical properties. For this purpose, the MMT powder sample was subjected to XRD analysis and the result is shown in Fig. 4. The X-ray diffraction pattern of MMT shows the major phase of montmorillonite whose main peak is at $2\theta = 19°$, 22°, 28°, 37°, and 53°. The presence of quartz at $2\theta = 23°$ and 29° is noted. A peak at $2\theta = 34°$ can be attributed, presumably, to calcite. The reflection at $2\theta = 32°$ on the MMT clay proves the presence of sodium feldspar [28].

Bragg's equation, $2d \sin\theta = n\lambda$, was used to calculate the basal spacing ($d_{001}$) of the MMT.

The characteristic $d_{001}$ diffraction peak for MMT in the 2θ region is located at 6.52°, $d_{001} = 13.54$ Å.

**Specific surface area (SSA) and cation exchange capacity (CEC).** Surface area and cation exchange capacity measurements of clay minerals are important for characterizing their bonding and swelling power, adsorptivity for polar compounds, and plasticity. Methylene blue (MB) spot and titration methods are widely used for SSA and CEC determination where they estimate them more accurately than other conventional methods. Following equations are used to calculate SSA and CEC, respectively [25]:

$$\mathrm{SSA} = \frac{m_{\mathrm{MB}}}{319.87} A_{\mathrm{V}} A_{\mathrm{MB}} \frac{1}{m_{\mathrm{s}}}, \quad (3)$$

$$\mathrm{CEC} = \frac{100}{m_{\mathrm{s}}} V_{\mathrm{cc}} N_{\mathrm{mb}}, \quad (4)$$

where $m_{\mathrm{MB}}$ is the mass of the adsorbed MB at the point of complete replacement, $m_{\mathrm{s}}$ is the mass of the clay specimen, 319.87 is the molecular weight of MB dye, $A_{\mathrm{V}}$ is Avogadro's number ($6.023 \times 10^{23}$/mol), $A_{\mathrm{MB}}$ is the area covered by one MB molecule, $V_{\mathrm{cc}}$ is the volume of the MB titrant, and $N_{\mathrm{mb}}$ is the normality of the MB (meq/mL). By substitution in Eqs. (3) and (4), it was found that the SSA and CEC of the MMT are 177 $m^2$/g and 94 meq/100 g, respectively. For comparison purposes, SSA is also measured by $N_2$ adsorption method (BET specific surface area) using a Quantachrome Monosorb®device (Quantachrome Instruments, Boynton Beach, Florida, USA) and it was found to be 75.5 $m^2$/g. This value is very small compared to that estimated by MB test due to the $N_2$ adsorption technique estimates only the external surface area rather than total surface area for swelling silicates.

**Thermogravimetric analysis (TGA).** The TGA and DTGA curves MMT are shown in Fig. 5. MMT displays two thermal degradation transitions. The first one occurs in the temperature range 100–350°C and is due to the vaporization of both the free water (i.e., the water sorbed on the external surfaces of crystals) and the water residing inside the interlayer space, forming hydration spheres around the exchangeable cation [26, 28]. The second transition is observed at higher temperatures (between 500 and 800°C) and is attributed to the structural water resulting from the dehydroxylation of clay OH units.

### *Adsorption Studies*

**The effect of contact time** on the adsorption of $Cd^{2+}$ ion onto MMT clay at 25°C and pH 6.1 is shown in Fig. 6. It can be seen that the adsorption of $Cd^{2+}$ occurred very quickly from the beginning of the experiment to the first 12 min, where the maximum adsorption of $Cd^{2+}$ onto clay was observed; it can be said that

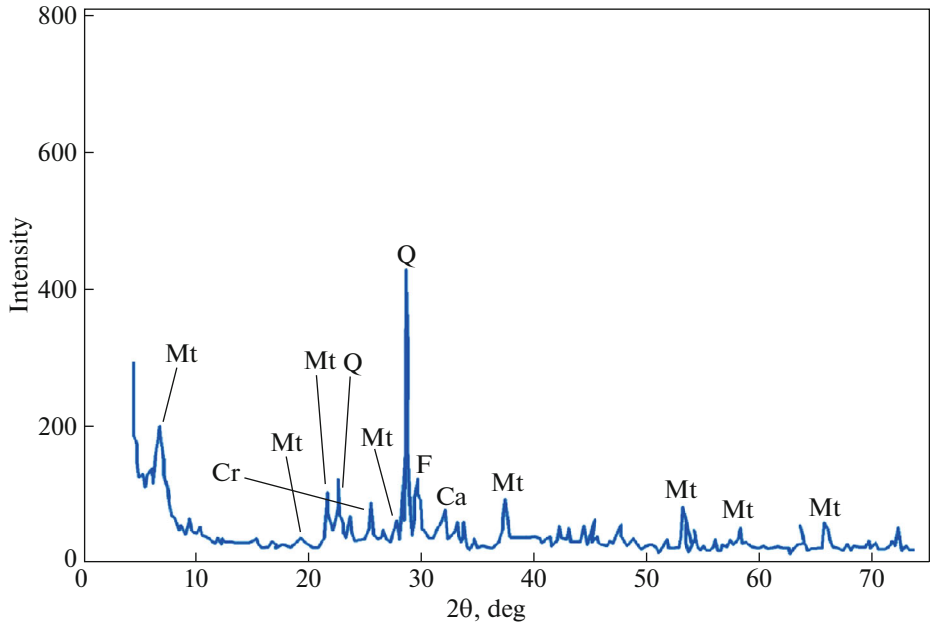


**Fig. 4.** XRD pattern of MMT; Mt—montmorillonite, Q—quartz, Cr—cristobalite, F—feldspar, Ca—calcite.

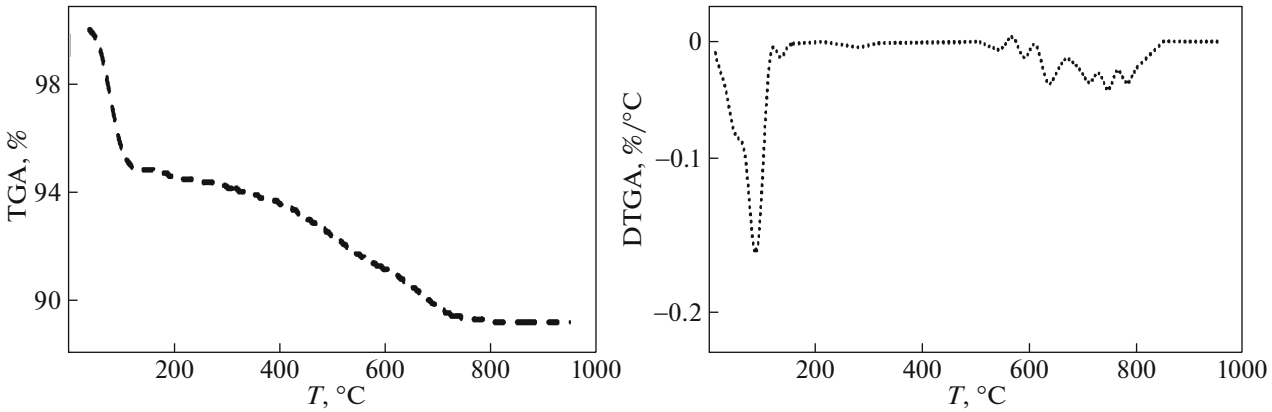


**Fig. 5.** TGA and DTGA curves of MMT.

beyond this there was almost no further increase in the adsorption. This was due to the decrease in the number of adsorption sites on the clay which gradually interacted with the metal ion [29]. Therefore, 12 min was selected as the optimum contact time for all further experiments.

In this study, 94.4% of $Cd^{2+}$, were adsorbed on the MMT clay when the equilibrium was reached in just 12 min. On the basis of this result, it can be observed that natural MMT clay can be used to remove this metal ion.

**Effect of initial concentration of $Cd^{2+}$** on adsorption capacity of MMT was investigated by varying initial concentration of $Cd^{2+}$ from 10 to 120 mg/L. For this study, pH, temperature, adsorbent dosage, and contact time have been fixed as 25°C, 0.2 g/20 mL, and 12 min. The results are presented in Fig. 7. An increase in $Cd^{2+}$ concentration accelerates the diffusion of $Cd^{2+}$ ions from solution to the adsorbent surface due to the increase in driving force of concentration gradient. Hence, the amount of adsorbed $Cd^{2+}$ at equilibrium increased from 0.98 to 10.44 mg/g as the $Cd^{2+}$ concentration is increased from 10 to 120 mg/L.

**Effect of initial pH** on the adsorption capacity of MMT for $Cd^{2+}$ was studied by varying solution pH from 1.5 to 11 at the adsorbent dosage of 0.2 g/20 mL using an initial $Cd^{2+}$ concentration of 100 mg/L. The pH range of 1.5–6.1 was chosen, as the precipitation of $Cd^{2+}$ is found to occur at pH ≥7 [30]. Variation of adsorption capacity of MMT for $Cd^{2+}$ ions with pH is shown in Fig. 8. It is evident that the adsorption of $Cd^{2+}$ ions on MMT is strongly dependent on the pH of the solution. The adsorption of $Cd^{2+}$ ions increases steadily with increase in initial pH from 1.5 to 6.1 and

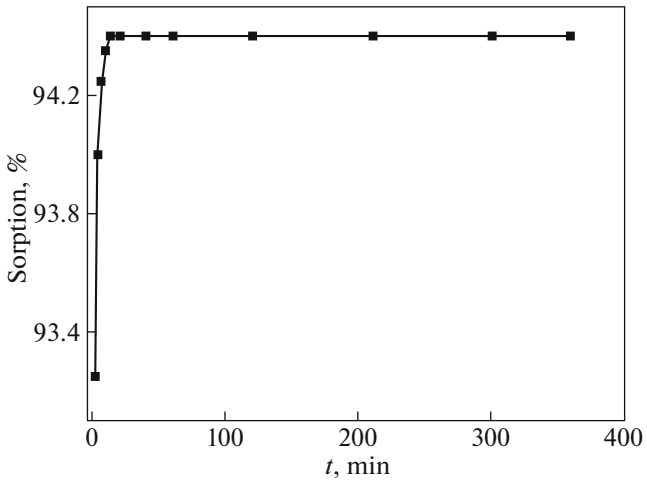


**Fig. 6.** Effect of contact time on adsorption capacity of MMT.

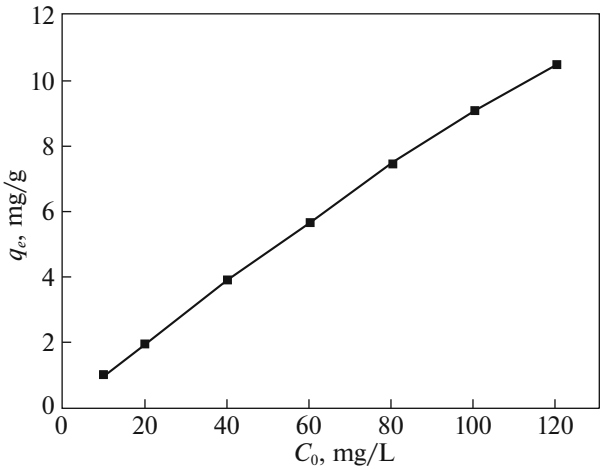


**Fig. 7.** Effect of initial concentration of $Cd^{2+}$ on adsorption capacity of MMT.

the maximum adsorption capacity of 9.4 mg/g is observed at pH 6.1 (natural pH of suspension).

The effect of pH can be explained considering the surface charge on the adsorbent material. At low pH values (pH 2–6), the low adsorption was explained due to increase in positive charge (protons) density on the surface sites and thus, electrostatic repulsion occurred between the metal ions ($M^{2+}$:$Cd^{2+}$) and the surface groups with positive charge (Si–$OH^{2+}$) on the surface as follows [31]:

$$-SiOH + H^+ \rightarrow -SiOH^{2+} + H^-. \quad (5)$$

In an alkaline medium (pH ≥7), the surface of kaolin clay becomes negatively charged and electrostatic repulsion decreases with raising pH due to reduction of positive charge density on the sorption surface thus resulting in an increase metal adsorption. This mechanism can be shown as follows [31]:

$$-SiOH + H^+ \rightarrow -SiO^- + H_2O, \quad (6)$$

$$-SiO^- + M^{2+} \rightarrow -SiOH^{2+}. \quad (7)$$

A similar theory was proposed in several works for metal adsorption on different adsorbents [30].

### *Adsorption Isotherm Models*

**Langmuir isotherm model** was applied to establish the relationship between the amount of $Cd^{2+}$ adsorbed onto MMT clay and its equilibrium concentration in aqueous solution. Langmuir adsorption isotherm [32] is applied to equilibrium adsorption assuming monolayer adsorption onto a surface with a finite number of identical sites and is represented in linear form:

$$\frac{C_e}{q_e} = \frac{1}{q_m K_L} + \frac{C_e}{q_m}, \quad (8)$$

where $q_e$ is the equilibrium adsorption capacity (mg/g), $C_e$ is the metal ions equilibrium concentration (mg/L); $K_L$ (L/g) and $q_m$ (mg/g) are Langmuir constant relating maximum monolayer coverage capacity and the enthalpy of adsorption, respectively. These constants are evaluated from slope and intercept of the linear plots of $C_e/q_e$ versus $C_e$, respectively (Fig. 9).

The Langmuir monolayer adsorption capacity of MMT clay was estimated as 12.30 mg/g (Table 2**)**. Based on the further analysis of Langmuir equation, the dimensionless parameter of the equilibrium adsorption intensity ($R_L$) can be expressed by:

$$R_L = \frac{1}{1 + K_L C_0}, \quad (9)$$

where $C_0$ (mg/L) is the initial $Cd^{2+}$ ions concentrations and $K_L$ (L/g) is Langmuir constant related to the energy of adsorption. The value of $R_L$ indicates the shape of the isotherms to be either unfavorable ($R_L > 1$), linear ($R_L = 1$), favorable ($0 < R_L < 1$) or

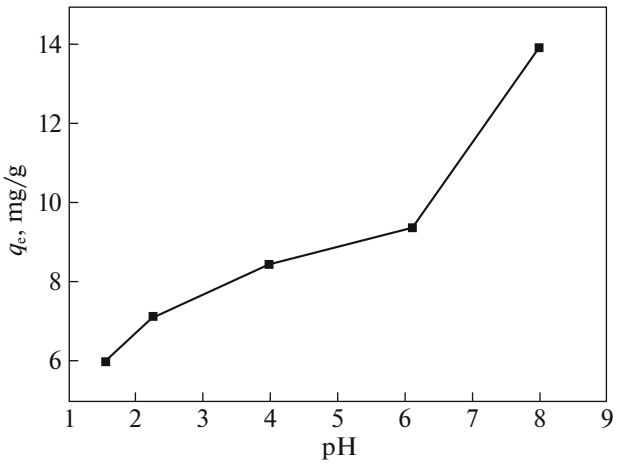


**Fig. 8.** Effect of pH on adsorption capacity of MMT.

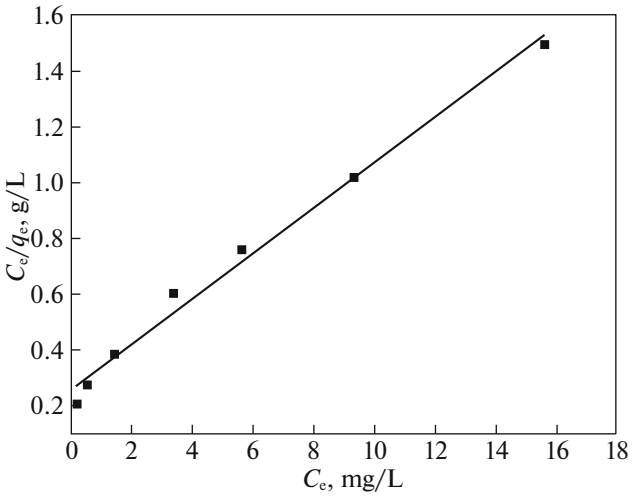


**Fig. 9.** Langmuir isotherm plot for adsorption of $Cd^{2+}$ on MMT.

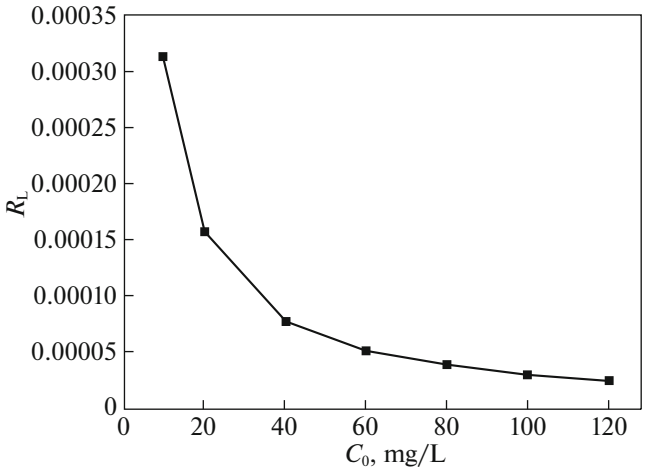


**Fig. 10.** Dependence of separation factor on initial $Cd^{2+}$ concentration.

irreversible ($R_L = 0$). The influence of isotherm shape on whether adsorption is favorable or unfavorable has been considered [33].

For a Langmuir type adsorption process, the isotherm shape can be classified by a dimensionless separation factor ($R_L$), given by Eq. (9). The calculated $R_L$ values as different initial $Cd^{2+}$ concentrations are shown in Fig. 10. It was observed that the value of $R_L$ in the range 0–1 confirmed that $Cd^{2+}$ adsorption is favorable process. Also lower $R_L$ values at higher initial $Cd^{2+}$ concentrations showed that adsorption was more favorable at higher concentrations. The degree of favorability is generally related to the irreversibility of the system, giving a qualitative assessment of the MMT–$Cd^{2+}$ interactions. The degrees tended toward zero (the completely ideal irreversible case) rather than unity (which represents a completely reversible case).

**Freundlich isotherm model.** The equilibrium data was also applied to the Freundlich adsorption isotherm [34], which is the earliest relationship known describing the adsorption equilibrium and is expressed in linear form by the following equation:

$$\log q_e = \log K_F + \frac{1}{n_F}\log C_e, \quad (10)$$

where $K_F$ and $n_F$ are Freundlich constants related to adsorption capacity and adsorption intensity, respectively. When $\log q_e$ is plotted against $\log C_e$, a straight line with slope $n_F$ and intercept $K_F$ is obtained (see Fig. 11). The intercept of the line, $K_F$, is roughly an indicator of the adsorption capacity and the slope, $n_F$, is an indication of adsorption intensity. The values obtained for the Freundlich variables for the adsorption of $Cd^{2+}$ ions are given in Table 2.

A relatively slight slope $n_F < 1$ indicates that adsorption intensity is good (or favorable) over the entire range of concentrations studied, while a steep slope ($n_F > 1$) means that adsorption intensity is good (or favorable) at high concentrations but much less at lower concentrations [35]. In the present study, the value of $n_F$ ($n_F = 1.83$) is greater than 1, indicating that the adsorption process is favorable. The $K_F$ value of the Freundlich equation also indicates that MMT has a high adsorption capacity for cadmium ions in aqueous solutions. The value of correlation coefficient ($R^2 = 0.980$) is also good. It can be said that Freundlich model fitted well.

**Adsorption kinetic models.** In an attempt to present the kinetic equation representing adsorption of $Cd^{2+}$ onto MMT clay, two kinds of kinetic models were used to test the experimental data. These are Lagergren first-order equation and second-order equation.

Lagergren first-order equation is the most popular kinetics equation. The form is

$$\frac{dq}{dt} = k_1(q_e - q_t). \quad (11)$$

After definite integration by applying the conditions $q_t = 0$ at $t = 0$ and $q_t = q_t$ at $t = t$, Eq. (11) becomes the following [36]:

$$\ln(q_e - q_t) = \ln q_e - k_1 t, \quad (12)$$

where $q_t$ (mg/g) is the amount of adsorption time $t$ (min); $k_1$ ($min^{-1}$), the rate constant of equation, and $q_e$

**Table 2.** Langmuir and Freundlich isotherm parameters for the adsorption of $Cd^{2+}$ on MMT

| Langmuir | | | Freundlich | | |
|---|---|---|---|---|---|
| $q_m$, mg/g | $K_L$, L/g | $R^2$ | $n_F$ | $K_F$ | $R^2$ |
| 12.30 | 0.31 | 0.987 | 1.83 | 2.69 | 0.980 |

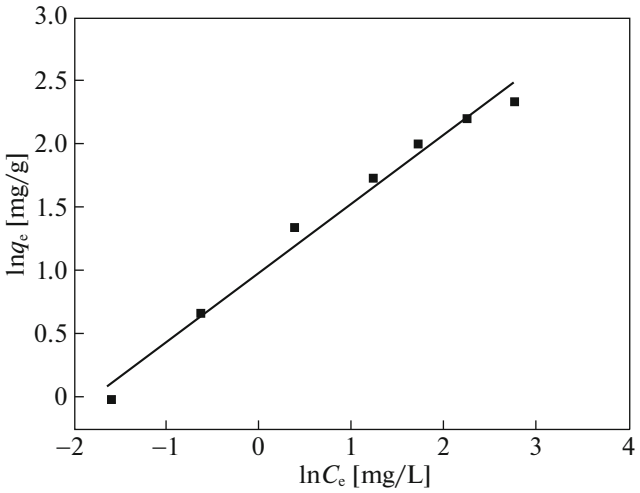


**Fig. 11.** Freundlich isotherm plot for adsorption of $Cd^{2+}$ on MMT.

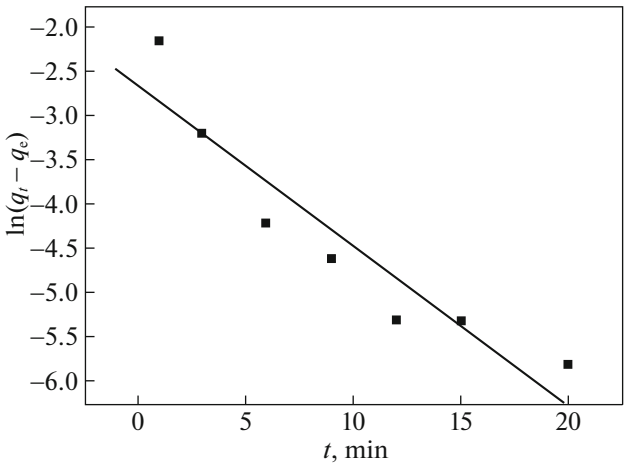


**Fig. 12.** Pseudo-first-order plot for adsorption of $Cd^{2+}$ on MMT.

(mg/g) is the amount adsorption equilibrium. The adsorption rate constant $k_1$, can be determined experimentally by plotting of ln $(q_e - q_t)$ versus $t$ (see Fig. 12).

The second-order equation is in the following form:

$$\frac{dq}{dt} = k_2(q_e - q_t)^2. \quad (13)$$

After definite integration by applying the conditions $q_t = 0$ at $t = 0$ and $q_t = q_t$ at $t = t$, Eq. (13) becomes the following [37]:

$$\frac{t}{q_t} = \frac{1}{k_2 q_e^2} + \frac{1}{q_e}t, \quad (14)$$

where $q_t$ (mg/g) is the amount of adsorption at the time $t$ (min), $k_2$ (g/(mg min)) is the rate constant of the second-order equation, and $q_e$ is the amount of adsorption equilibrium (mg/g).

$k_2$ and $q_e$ can determined experimentally by plotting of $t/q_t$ versus $t$ (Fig. 13).

Based on the correlation coefficients presented in Table 2, the adsorption of $Cd^{2+}$ onto MMT was best described by the second order equation. A good agreement with this adsorption model was confirmed by the similar values of $q_e$ experimental and $q_e$ calculated. Many studies reported Lagergren's first-order equation does not fit well to the initial stages of the adsorption processes [38]. The first-order kinetic process has been used for reversible reaction with an equilibrium being established between liquid and solid phases. In many cases, the second-order equation correlates well to the adsorption studies [39].

The best fit to the pseudo-second order kinetic indicated that the adsorption mechanism depended on the adsorbate and adsorbent.

**Thermodynamics of adsorption.** Adsorption experiments to study the effect of temperature were carried out from 25 to 60°C at optimum pH value of 6.1 and adsorbent loading of 0.1 g/L. The contact time for adsorption was maintained at 12 min. The variation in the extent of adsorption with respect to temperature has been explained based on thermodynamic parameters viz. free energy change ($\Delta G$), enthalpy change ($\Delta H$), and entropy change ($\Delta S$), which were determined using the following equations [40]:

$$K_d = \frac{q_e}{C_e}, \quad (15)$$

$$\ln K_d = -\frac{\Delta G}{RT} = \frac{\Delta S}{R} - \frac{\Delta H}{RT}, \quad (16)$$

$$\Delta G^\circ = \Delta H - T\Delta S, \quad (17)$$

where $\ln K_d$ was plotted against $1/T$, (Fig. 14), a straight line with the slope of $\Delta H/T$ and intercept of $\Delta S/R$ were obtained. The values of $\Delta H$ and $\Delta S$ were obtained from the slope and intercept of the Van't

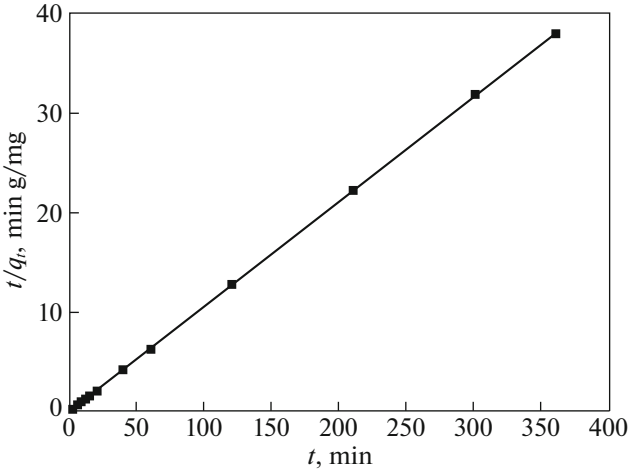


**Fig. 13.** Pseudo-second-order plot for adsorption of $Cd^{2+}$ on MMT.

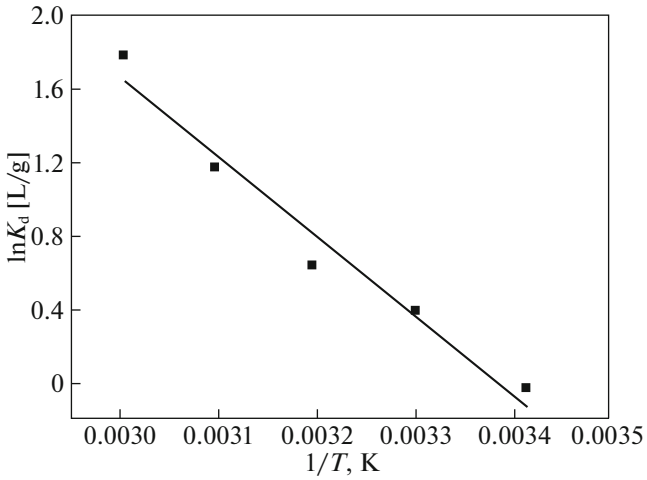


**Fig. 14.** Plot of $\ln K_d$ verses $1/T$ for adsorption $Cd^{2+}$ on MMT.

Hoff plots. The thermodynamic parameters for the adsorption process are given in Table 3.

It is clear that positive value of $\Delta H$ suggested the endothermic nature of the adsorption and the negative value of $\Delta G$ indicated the spontaneous nature of the adsorption process. Generally, the change in adsorption enthalpy for physisorption is in the range of −20 to 40 kJ/mol, but chemisorption is between −400 and −80 kJ/mol [40]. The value of adsorption heat showed that physical adsorption took place in the adsorption of $Cd^{2+}$ ion on MMT.

The slightly positive $\Delta S$ value showed the increased randomness at the solid/solution interface during the adsorption process. The adsorbed water molecules, which were displaced by the adsorbate species, gained more translational energy than was lost by the adsorbate ions, thus allowing the prevalence of the randomness in the system. Enhancement of the adsorption capacity at higher temperatures may be attributed to the enlargement of pore size and/or activation of the adsorbent surface [41].

**Table 3.** Thermodynamic parameters

| −ΔG, kJ/mol | | | | | ΔH, kJ/mol | ΔS, J/(mol K) | $R^2$ |
|---|---|---|---|---|---|---|---|
| 25°C | 30°C | 40°C | 50°C | 60°C | | | |
| 0.35 | 0.96 | 2.16 | 3.32 | 4.53 | 35.43 | 0.13 | 0.965 |

**Table 4.** Adsorption capacities ($q_e$) of various adsorbents studied for $Cd^{2+}$ removal

| Adsorbent | $q_e$, mg/g | Reference |
|---|---|---|
| Montmorillonite | 12.300 | Present study |
| Boa Vista, Brazil | 2.470 | [42] |
| Activated carbon | 10.030 | [43] |
| Untreated *Pinus sylvestris* bark | 8.690 | [44] |
| Treated *Pinus sylvestris* bark | 9.770 | [45] |
| Grain-less stalk of corn | 7.300 | [46] |

**Comparison of MMT clay with various adsorbents for $Cd^{2+}$ removal.** The adsorption capacity of the MMT clay in the removal of $Cd^{2+}$ was compared with those of other adsorbents reported in literature and the values of adsorption capacities were presented in Table 4. The values are reported in the form of monolayer adsorption capacity. The experimental data of the present investigation was comparable with the reported values. The MMT clay had a high adsorption capacity as comparable with that of the other adsorbent. Therefore, considering the low cost of this natural adsorbent, it can be used as an alternative material to minimize the concentration of $Cd^{2+}$ in wastewater.

## CONCLUSIONS

The results of present investigation show that MMT, low cost material, has suitable adsorption capacity with regard to the removal of cadmium ions from aqueous solutions. The amount of adsorbed $Cd^{2+}$ ions increased with increase in initial concentration of adsorbat, pH and temperature. Experimental results were approximated with Langmuir and Freundlich isotherms. In addition to higher values of correlation coefficients, monolayer capacities ($q_m$) determined from Langmuir isotherm and adsorption intensity ($n_F$) determined from Freundlich isotherm indicate appropriateness of Langmuir and Freundlich for cadmium metal. Pseudo-second-order reaction kinetic has provided a realistic description for removal of $Cd^{2+}$ with similar values of $q_e$ calculated and $q_e$ experimental, whereas in the first-order kinetic the difference between these values is large. The correlation coefficient was also higher in pseudo-second-order kinetic.

The enthalpy change for the adsorption process was indicative of the endothermic nature of adsorption. The dimensionless separation factor ($R_L$) showed that MMT can be used for removal of cadmium ions from aqueous solutions. The results of this research were compared to the published data in the same field, and found to be in agreement with most of them. The batch design may be useful for environmental technologist in designing treatment plants for metal removal from wastewaters.

## REFERENCES

1. L. S. Kostenko, I. I. Tomashchuk, T. V. Kovalchuk, et al., Appl. Clay Sci. **172**, 49 (2019).
2. K. Tohdee and L. Kaewsichan, J. Environ. Chem. Eng. **6**, 2821 (2018).
3. K. Jlassi, R. Abidi, M. Benna, et al., Appl. Clay Sci. **161**, 15 (2018).
4. P. Dipak, Ann. Agrar. Sci. **15**, 278 (2017).
5. D. Ouyang, Y. Zhuo, L. Hu, et al., Minerals **9**, 291 (2019).

6. F. P. Fato, D. Li, Li Zhao, et al., ACS Omega **4**, 7543 (2019).
7. M. Kapahi and S. Sachdeva, J. Health Pollut. **9**, 191203 (2019).
8. K. C. Khulbe and T. Matsuura, Appl. Water Sci. **8**, 19 (2018).
9. R. Valavala, J. Sohn, J. Han, et al., Environ. Eng. Res. **16**, 205 (2011).
10. M. A. Kamaruddin, N. Ismail, and U. N. Osman, Appl. Water Sci. **9**, 141 (2019).
11. R. Bisht, M. Agarwal, and K. Singh, Interdiscipl. Environ. Rev. **18**, 124 (2017).
12. M. K. Uddin, Chem. Eng. J. **308**, 438 (2017).
13. M. Fronczak, K. Pyrzyńska, A. Bhattarai, et al., Int. J. Environ. Sci. Technol. **16**, 7921 (2019).
14. M. Irannajad, H. K. Haghighi, and M. Soleimanipour, Physicochem. Probl. Miner. Process. **52**, 894 (2016).
15. L. Khezamia, K. K. Tahaa, and E. Amamic, Desalin. Water Treatm. **62**, 346 (2016).
16. E. Sahar et al., Radiochim. Acta **105**, 43 (2017).
17. M. A. Tahoon, S. M. Siddeeg, N. S. Alsaiari, et al., Processes **8**, 645 (2020).
18. R. Baby, B. Saifullah, and M. Z. Hussein, Nanoscale Res. Lett. **14**, 341 (2019).
19. S. Gu et al., Environ. Chem. Lett. **17**, 629 (2019).
20. M. K. Uddin, Res. J. Chem. Environ. **308**, 438 (2017).
21. S. A. Hamid, M. Shahadat, and S. Ismail, Appl. Clay Sci. **149**, 79 (2017).
22. J. N. Putro, S. P. Santoso, S. Ismadji, et al., Microporous Mesoporous Mater. **246**, 166 (2017).
23. T. Ngulube, J. R. Gumbo, V. Masindi, et al., J. Environ. Manage. **191**, 35 (2017).
24. R. Fabryanty et al., J. Environ. Chem. Eng. **5**, 5677 (2017).
25. Y. Yukselen and A. Kaya, Eng. Geol. **102**, 38 (2008).
26. S. Boudjemaaa and B. Djellouli, Russ. J. Appl. Chem. **87**, 1464 (2014).
27. N. Sarier and E. Onder, Thermochim. Acta **510**, 113 (2010).
28. S. Boudjemaa, Rev. Roum. Chim. **64**, 35 (2019).
29. Z. H. Siahpoosh and M. J. Soleimani, Water Environ. Nanotechnol. **2**, 39 (2017).
30. L. S. G. Galindo et al., Mater. Res. **16**, 515 (2013).
31. L. S. Kostenko, I. I. Tomashchuk, T. V. Kovalchuk, et al., Appl. Clay Sci. **172**, 49 (2019).
32. I. Langmuir, J. Am. Chem. Soc. **40**, 1361 (1918).
33. J. N. Wekoye, W. C. Wanyonyi, P. T. Wangila, et al., Environ. Chem. Ecotoxicol. **2**, 24 (2020).
34. H. M. F. Freundlich, Zeitschr. Phys. Chem. (Leipzig) **57**, 385 (1906).
35. K. S. Obayomi and M. Auta, Heliyon **5**, 2799 (2019).
36. N. Khandelwal, N. Singh, E. Tiwaria, et al., R. Soc. Chem. **9**, 11160 (2019).
37. Y. A. El-Damarawy et al., Nat. Sci. **15** (12), 154 (2017).
38. K. Wu, Y. Li, T. Liu, et al., Environ Sci. Pollut. Res. **26**, 17632 (2019).
39. Q. Zhang, B. Lin, J. Hong, et al., Water Sci. Technol. **75**, 587 (2017).
40. Z. Melichová and A. Luptáková, Desalin. Water Treatm. **57**, 5025 (2016).
41. S. Siddiqui, G. Rathi, and S. A. Chaudhry, J. Mol. Liq. **264**, 275 (2018).
42. L. H. G. Chaves and G. A. Tit, Rev. Cien. Agronom. **42**, 278 (2011).
43. H. Sharififard, M. Nabavinia, and M. Soleimani, Adv. Environ. Technol. **4**, 215 (2016).
44. Y. Ding, D. Jing, H. Gong, et al., Bioresour. Technol. **114**, 20 (2012).
45. N. Azouaou, Z. Sadaoui, A. Djaafri, et al., J. Hazard Mater. **184**, 126 (2010).
46. F. Okeola, E. Odebunmi, F. Nwosu, et al., Nig. J. Pure Appl. Sci. **30**, 2955 (2017).